Fluid–Fluid Membrane Microheterogeneity: A Fluorescence Resonance Energy Transfer Study

Luís M. S. Loura,*† Aleksandre Fedorov,*‡ and Manuel Prieto*

*Centro de Química-Física Molecular, Instituto Superior Técnico, P-1049-001 Lisboa, Portugal, †Departamento de Química, Universidade de Évora, P-7000-671 Évora, Portugal, and ‡On leave from the Vavilov Optical Institute, St. Petersburg, Russia

ABSTRACT Large unilamellar vesicles of dimyristoylphosphatidylcholine/cholesterol mixtures were studied using fluorescence techniques (steady-state fluorescence intensity and anisotropy, fluorescence lifetime, and fluorescence resonance energy transfer (FRET)). Three compositions (cholesterol mole fraction 0.15, 0.20, and 0.25) and two temperatures (30 and 40°C) inside the coexistence range of liquid-ordered (l_o) and liquid-disordered (l_d) phases were investigated. Two common membrane probes, *N*-(7-nitrobenz-2-oxa-1,3-diazol-4-yl)-dimyristoylphosphatidylethanolamine (NBD-DMPE) and *N*-(lissamine™-rhodamine B)-dimyristoylphosphatidylethanolamine (Rh-DMPE), which form a FRET pair, were used. The l_o/l_d partition coefficients of the probes were determined by individual photophysical measurements and global analysis of time-resolved FRET decays. Although the acceptor, Rh-DMPE, prefers the l_d phase, the opposite is observed for the donor, NBD-DMPE. Accordingly, FRET efficiency decreases as a consequence of phase separation. Comparing the independent measurements of partition coefficient, it was possible to detect very small domains (<20 nm) of l_o in the cholesterol-poor end of the phase coexistence range. In contrast, domains of l_d in the cholesterol-rich end of the coexistence range have comparatively large size. These observations are probably related to different processes of phase separation, nucleation being preferred in formation of l_o phase from initially pure l_d, and domain growth being faster in formation of l_d phase from initially pure l_o.

INTRODUCTION

Cholesterol is a major component of mammalian cells, and its action upon the physical properties of lipid bilayers has been studied actively in the last three decades. Some consensual results have emerged from these efforts, particularly that cholesterol concentrations of approximately 10–30% produce phase separation above the main transition temperature of dimyristoylphosphatidylcholine (DMPC) and dipalmitoylphosphatidylcholine (DPPC). The monotetic phase diagram for the DMPC/cholesterol mixture is shown in Fig. 1 (Almeida et al., 1992). The two coexisting phases, the so-called liquid-ordered (l_o) and liquid-disordered (l_d) phases, have been thoroughly characterized in terms of physical properties. Although l_d resembles the pure lipid fluid, l_o has intermediate properties between those of pure phospholipid fluid and gel. The notable effects of cholesterol include condensation of area/lipid molecule (e.g., Smaby et al., 1997), reduction in passive permeability of the bilayer (e.g., Xiang and Anderson, 1997), increase in orientational order of the phospholipid acyl chains (e.g., Lafleur et al., 1990) and increase in bending elasticity (e.g., Méléard et al., 1997), relative to the values in pure phospholipid fluid membranes. McMullen and McElhaney (1996) have recently reviewed this field and pointed out that, despite all research on the effect of cholesterol on phospholipid bilayers, a complete molecular-level rationalization of these changes is still lacking.

The usual hypotheses of cholesterol molecular organization at high molar fractions involve formation of sterol/phospholipid complexes of a given stoichiometry, most commonly 1:1. Vanderkooi (1994) performed energy-minimization calculations for an equimolar DMPC/cholesterol mixture and obtained two relative minima, the lowest of which corresponds to nonidentical nearest neighbors. Subsequent molecular dynamics simulations have used these packing structures as starting points and have generally confirmed the observed physical effects of cholesterol on DMPC/cholesterol (Gabdoulline et al., 1996) and DPPC/cholesterol (Smondyrev and Berkowitz, 1999) bilayers. However, as pointed out by the latter authors, this choice of initial arrangement is certainly not unique. Moreover, although the recent progress in computational techniques has led to interesting accordance between observed and predicted physical properties for either very high (1:1; Gabdoulline et al., 1996, Smondyrev and Berkowitz, 1999) or very low (1:9 or 1:8; Robinson et al., 1995; Tu et al., 1998; Smondyrev and Berkowitz, 1999) cholesterol:phospholipid ratios, for which a sole phase (l_o or l_d, respectively) is expected, little advance has been made recently regarding the intermediate composition range, for which domains of l_o and l_d phases are expected to coexist. This region of the phase diagram is, however, especially important as a study model of heterogeneity in fluid biological membranes. This latter phenomenon has considerable biological relevance, because the existence of small membrane domains can influence membrane functions by concentrating some spe-

Received for publication 25 April 2000 and in final form 1 November 2000.

Address reprint requests to Luis M. S. Loura, Inst. Superior Tecnico, Centro de Quimica-Fisica Molecular, P-1049-001 Lisboa, Portugal. Tel.: +351-21-8419248; Fax: +351-21-8464455; E-mail: pclloura@alfa.ist.utl.pt.

0006-3495/01/02/776/13 $2.00

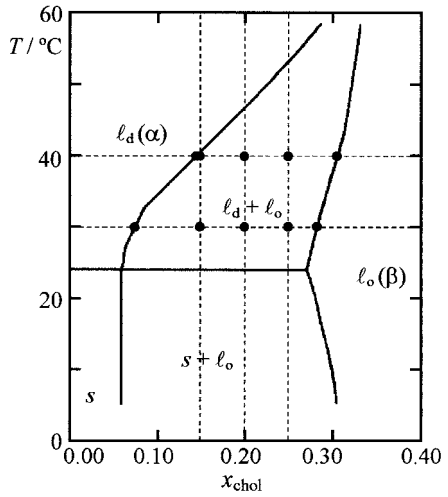

FIGURE 1 Phase diagram of DMPC/cholesterol (Almeida et al., 1992). The points indicate the mixtures and temperatures addressed in this study.

cies in particular membrane regions, or rather by excluding molecules from them (Edidin, 1997).

In this regard, several experimental techniques have been used in the experimental study of phosphatidylcholine/cholesterol mixtures. DSC (Mabrey et al., 1978; Vist and Davis, 1990) is useful regarding the study of non-ideality of lipid mixtures, but does not give topological information. A number of spectroscopic techniques, such as ^{2}H-NMR (e.g., Vist and Davis, 1990), ESR (e.g., Sankaram and Thompson, 1990, 1991) and steady-state and time-resolved fluorescence (e.g., Lentz et al., 1980; Mateo et al., 1995) are also sensitive to the environment surrounding the spectroscopic probes, but are not usually informative regarding the lateral organization of each phase. Fluorescence recovery after photobleaching has been used to estimate phase microdomain sizes in multibilayers containing cholesterol, DMPC and distearoylphosphatidylcholine (DSPC; Almeida et al., 1993). However, these values were obtained only for coexistence of one solid and one liquid phase, and not in the (probably most relevant to biological membranes) fluid–fluid coexistence region.

Fluorescence resonance energy transfer (FRET; reviewed in Van der Meer et al., 1994; Lakowicz, 1999) is a photophysical process that causes quenching of the fluorescence of one species (the donor), by nonradiative transfer of its excitation energy to another species (the acceptor), which absorption spectrum overlaps the emission spectrum of the donor. The strong dependence (sixth power) of the FRET rate on the intermolecular distance has led to its wide use in biochemistry in the last three decades as a "spectroscopic ruler" for determination of distances in the 1–10 nm range (Stryer, 1978). If, instead of an isolated donor/acceptor pair at a single defined distance, there is a distribution of donor and acceptor molecules in three-dimensional space or in a plane (the geometry relevant for membranes), donor fluorescence becomes dependent on the acceptor concentration surrounding the donors.

In this paper, we show that, for a microheterogeneous binary lipid system, by the means of simple relationships, it is possible to extract information on the partition of both donor and acceptor probes in each environment, and on the lipid mixture phase diagram boundaries, from the parameters of the donor fluorescence decay in presence of acceptor. Additionally, using Monte-Carlo simulations together with global analysis of fluorescence decays, we show that deviations to the theoretical decay laws (derived assuming large domain sizes) can provide unique information on the size of the lipid domains. This approach is then carried out for three DMPC/cholesterol mixtures (cholesterol mole fractions $x_{chol} = 0.15$, $x_{chol} = 0.20$, $x_{chol} = 0.25$) for two temperatures within the fluid–fluid phase coexistence range (30 and 40°C; see Fig. 1). Labeled phospholipids were selected as fluorescent probes. *N*-(7-nitrobenz-2-oxa-1,3-diazol-4-yl)-dimyristoylphosphatidylethanolamine (NBD-DMPE) was used as FRET donor, and *N*-(lissamine™-rhodamine B)-dipalmitoylphosphatidylethanolamine (Rh-DMPE; acceptor) was the FRET acceptor.

THEORY

Consider a planar system of two infinite separated phases, labeled 1 and 2. If the fluorescence decay of the donor in each phase is a single exponential,

$$\rho_{Di}(t) = \exp(-t/\tau_i), \tag{1}$$

then, upon incorporation of acceptor probe with a concentration of n_i molecules/area unit, the decay becomes complex (e.g., Hauser et al., 1976),

$$\rho_{DAi}(t) = \rho_{Di}(t)\exp(-c_i t^{1/3}), \tag{2}$$

where

$$c_i = \Gamma(\tfrac{2}{3}) \cdot n_i \cdot \pi \cdot R_{0i}^2 \cdot \tau_i^{-1/3}. \tag{3}$$

In this equation, R_{0i} is the Förster critical distance for phase i, and Γ is the complete gamma function. Considering the whole biphasic system, the donor decay in the absence of acceptor is now

$$\rho_D(t) = A_1\rho_{D1}(t) + A_2\rho_{D2}(t), \tag{4}$$

where A_i is proportional to the number of donor molecules in phase i, and, in presence of acceptor, the decay law becomes

$$\rho_{DA}(t) = A_1\rho_{DA1}(t) + A_2\rho_{DA2}(t), \tag{5}$$

or, equivalently,

$$\rho_{DA}(t) = A_1\exp(-t/\tau_1)\exp(-c_1 t^{1/3}) + A_2\exp(-t/\tau_2)\exp(-c_2 t^{1/3}). \tag{6}$$

This equation shows clearly that the decay of donor fluorescence in the presence of acceptor contains information on the amounts of donor and acceptor probes within each phase of the system. For biexponential decay of donor within each phase, and bilayer (rather than planar; Davenport et al., 1985) geometry of FRET, Eqs. 4 and 5 are still valid, with the following alterations:

$$\rho_{Di}(t) = \exp(-t/\tau_{1i}) + q_i\exp(-t/\tau_{2i}) \tag{7}$$

$$\rho_{DAi}(t) = \rho_{Di}(t) \cdot \exp\left\{-c_i \cdot t^{1/3} - \frac{2\,c_i}{\Gamma(2/3) \cdot b_i} \cdot \int_0^1 [1 - \exp(-t\, b_i^3\alpha^6)]\alpha^{-3}\, d\alpha\right\}, \tag{8}$$

where τ_{ji} are the different donor lifetime components in phase i, q_i is their amplitude ratio, and

$$b_i = (R_{0i}/d_i)^2/\bar{\tau}_i^{1/3}. \tag{9}$$

In this latter definition, R_{0i} and d_i are, respectively, the Förster critical distance for FRET and the bilayer width in phase i, and

$$\bar{\tau}_i = (\tau_{1i} + q \cdot \tau_{2i})/(1 + q_i). \tag{10}$$

The distribution of probes between two lipid phases, 1 and 2 (the actual type of phases involved—e.g., gel, fluid, liquid-ordered—is not important in the following) is commonly described on the basis of a partition equilibrium,

$$(\text{probe})_1 \rightleftharpoons (\text{probe})_2. \tag{11}$$

The partition coefficient of this probe between phases 1 and 2 is given by (e.g., Davenport, 1997)

$$K_p = (P_2/X_2)/(P_1/X_1). \tag{12}$$

In this equation, P_1 is the probe mole fraction in lipid phase 1, and X_1 is the lipid phase 1 mole fraction (therefore, $P_2 = 1 - P_1$ and $X_2 = 1 - X_1$). Combining Eqs. 6 and 12, it is easy to show that the partition coefficients of donor (K_{pD}) and acceptor (K_{pA}) probes can be calculated straightforwardly from the FRET decay parameters,

$$K_{pD} = (A_2/X_2)/(A_1/X_1), \tag{13}$$

$$K_{pA} = (c_2 \cdot a_2)/(c_1 \cdot a_1), \tag{14}$$

where a_i is the area per lipid molecule in phase i (usually known from X-ray diffraction studies; a good collection is given in Marsh, 1990).

Consider now a composition x (which represents the overall mole fraction of the lipid component that predominates in phase 2) that, at a given temperature T, corresponds to a (x, T) point within the phase 1/phase 2 coexistence range (note that this discussion is independent of the actual shape of the hypothetical phase diagram); let the phase coexistence boundaries at this temperature be x_1 ($X_2 = 0$) and x_2 ($X_1 = 1$). For the (x, T) point, X_1 and X_2 can be easily calculated from the lever rule

$$X_1 = (x_2 - x)/(x_2 - x_1) \tag{15}$$

$$X_2 = 1 - X_1 = (x - x_1)/(x_2 - x_1) \tag{16}$$

Now consider that the phase diagram for the lipid mixture is unknown. Let then F be the overall acceptor mole fraction (acceptor moles/total moles; it is an experimentally accessible amount), and let F_1 and F_2 be the acceptor mole fractions within each phase. F_1 (acceptor molecules in phase i/total lipid molecules in phase i) and n_i (acceptor molecules in phase i/area of phase i) are related according to

$$F_i = n_i a_i. \tag{17}$$

Combining Eqs. 3 and 17, one obtains the relationship between F_i and c_i,

$$F_i = \frac{c_i a_i}{\Gamma(2/3)\pi R_{0i}^2 \tau_i^{1/3}}. \tag{18}$$

Once both F_i are computed, from the acceptor mass balance equation,

$$F = F_2(1 - X_1) + F_1 \cdot X_1, \tag{19}$$

it is easy to calculate X_1 and X_2, even for an unknown phase diagram.

In this situation, if, at a given temperature, X_1 are known for two points, A(x_A, T) and B(x_B, T), which are known to be located inside the phase coexistence range, one obtains a system of two linear equations, which unknowns, x_1 and x_2, are given by

$$x_1 = (x_A \cdot X_{2B} - x_B \cdot X_{2A})/(X_{1A} - X_{1B}), \tag{20}$$

$$x_2 = (x_B \cdot X_{1A} - x_A \cdot X_{1B})/(X_{1A} - X_{1B}), \tag{21}$$

which allows one to calculate the compositions of phases 1 and 2 at that temperature from time-resolved FRET data. If this procedure is repeated for several temperatures, the phase diagram is obtained.

SIMULATIONS

The preceding considerations refer to an infinite-phase binary lipid mixture (that is, one in which the domains of phase i are $\gg R_{0i}$). To study their applicability to microheterogeneous mixtures in which the size of the domains is only a few times larger than the Förster distance (i.e., typically $<$50 nm), we carried out Monte-Carlo simulations. After assuming a shape and a size for the domains of the least abundant phase (dispersed inside the complementary phase), and the X_1 and X_2 values, their locations were generated randomly (with the restriction of nonoverlap of

different domains). Suitable K_{pD} and K_{pA} values were then chosen a priori. Finally, chosen numbers of donors and acceptors were distributed inside and outside the domains, according to their partition coefficient values. The probe distribution within each phase was random. A triangular lattice of $10^3 \times 10^3$ molecules was considered.

The hypothetical system had phase compositions $x_1 = 0.08$ and $x_2 = 0.72$ at a given temperature, and two different values for X_1 were assumed: 0.50 (which corresponds to a global composition $x = 0.40$; in this case, domains of phase 1 dispersed in phase 2 were generated) and 0.80 (which corresponds to a global composition $x = 0.21$; in this case, domains of phase 2 dispersed in phase 1 were generated). For each X_1 value, two different sizes of square domains were considered: 400 (20×20) molecules and 2500 (50×50) molecules. These domain sizes were chosen to be of the order of magnitude of those estimated by Sankaram et al. (1992) for a dilauroylphosphatidylcholine/distearoylphosphatidylcholine mixture (which exhibits gel/fluid phase coexistence). Obviously, a uniform domain size distribution is very unlikely. However, although the FRET decays are undoubtedly affected by the domain size, it is, at this point, impossible to recover multiple parameters of a nonuniform domain size distribution of a given family from experimental data, hence this model restriction. For each of these domain sizes, the values $K_{pD} = 1.00$ and $K_{pA} = 1.00$, 2.00, and 0.50 were considered. A total of 12 simulations was run, each with different K_p, domain size, and phase ratio. For the sake of brevity, only the characterization of the simulations with $X_1 = 0.50$ is given as example in Table 1. Each lattice location represented a molecule with 9-Å diameter. $N_D = 2 \times 10^3$ donors and $N_A = 5 \times 10^3$ acceptors were distributed in each simulation run. Donor lifetimes (typical dye lifetimes in fluid and gel lipid phases, respectively; Davenport, 1997) were $\tau_1 = 0.8$ ns and $\tau_2 = 1.32$ ns. $R_{01} = 47.2$ Å and $R_{02} = 50.1$ Å were considered for all simulations. For a donor j, located in phase i, the decay law is given by (Förster, 1949)

$$\rho_j(t) = \exp\left(-\frac{t}{\tau_i}\right)\prod_{k=1}^{N_A}\exp\left[\left(-\frac{t}{\tau_i}\right)\left(\frac{R_{0i}}{R_{jk}}\right)^6\right], \qquad (22)$$

where R_{jk} is the distance between donor j and acceptor k (for the calculation of this distance in a triangular lattice, see Snyder and Freire, 1982). We assume that there is a single R_0 parameter for every (donor in phase i, acceptor in either phase) pair (this condition is met in the dynamic orientational regime; note that the spectral overlap is usually phase independent) and neglect energy migration among donors (this can be experimentally achieved choosing a donor with no absorption/emission overlap or using low donor concentration). Periodic boundary conditions are used in the calculation of $\rho_j(t)$. The macroscopic decay is obtained by averaging over donors:

$$i_{DA}(t) = \frac{1}{N_D}\sum_{j=1}^{N_D}\rho_j(t). \qquad (23)$$

The generated decays were then convoluted with an experimental instrumental response function, and Poisson noise was added to them. They were then analyzed using Eq. 6 and software based on the Marquardt algorithm (Marquardt, 1963). Each FRET decay thus generated was analyzed globally together with an "experimental" (obtained from Eq. 4, after convolution and adding of Poisson noise) donor decay, for the lifetime parameters to be better recovered. Statistically acceptable fits were obtained for all simulations (global $\chi^2 < 1.1$). From the recovered c_i and A_i parameters, K_{pD}, K_{pA}, X_1, x_1, and x_2 were calculated from Eqs. 13–14 and 18–21. The values thus obtained are represented in the lower part of Table 1, for the simulations with $X_1 = 0.50$ (the simulations with $X_1 = 0.80$ resulted in identical trends).

As is shown in Table 1, for simulations 1 and 4 ($K_{pA} = 1.00$), the values recovered for c_1 and c_2 are virtually identical, as expected. The recovered K_{pA} is very close to 1.00. For all other simulations, K_{pA} was given the input value 2.0 (simulations 2 and 5) or 0.5 (simulations 3 and 6). In these cases, the highest c value (c_1 for $K_{pA} = 0.5$, c_2 for $K_{pA} = 2.0$) is always underestimated, whereas the lowest c value (c_2 para $K_{pA} = 0.5$, c_1 for $K_{pA} = 2.0$) is consistently overestimated. This is due to the small domain size: many of the donors located in phase 1 are sensitive to acceptors in phase 2, and conversely for the donors located in phase 2. This effect is more pronounced for the domain phase than for the continuous phase, especially when the former is more abundant.

TABLE 1 Input parameters for typical FRET Monte-Carlo simulations, and recovered parameters after their analysis

Run	1	2	3		4	5	6
Input parameters							
x_1				0.08			
x_2				0.72			
K_{pD}				1.00			
Size*		20×20				50×50	
x				0.21			
X_1				0.50			
K_{pA}	1.00	2.00	0.50		1.00	2.00	0.50
c_1	0.73	0.49	0.97		0.73	0.49	0.97
c_2	0.73	0.97	0.49		0.73	0.97	0.49
Recovered parameters							
c_1	0.71	0.63	0.89		0.74	0.49	0.96
c_2	0.68	0.80	0.57		0.68	0.92	0.51
X_1	—	0.41	0.50		—	0.56	0.51
K_{pD}	—	0.91	1.27		—	0.78	0.97
K_{pA}	0.96	1.27	0.64		0.92	1.88	0.53
x_1	—	0.04	0.17		—	0.08	0.08
x_2	—	0.65	0.63		—	0.65	0.71

The domain phase is denoted by the index "1".
*Size refers to the number of molecules of the domains.

As a consequence of these deviations, the K_{pA} values are always closer to unity than expected (between 1.0 and 2.0 for simulations 2 and 5 in Table 1; between 0.5 and 1.0 for simulations 3 and 6). In contrast, the parameters are consistently recovered with a smaller error when the domain size increases from 400 molecules ($\sim$3.5 R_0; simulations 2 and 3) to 2500 molecules ($\sim$9 R_0; simulations 5 and 6), as the system approaches the "infinite separated phases" hypothesis. In any case, even for the simulations in which the domain size is 400 molecules, the accuracy is relatively satisfactory, even for the phase diagram limit compositions (x_1 and x_2). Therefore, this method compares well with established procedures such as NMR difference spectroscopy (e.g., Vist and Davis, 1990). Some of the above equations of our method are reminiscent of NMR difference spectroscopy (both methods are based on the lever rule), but there are important differences, which arise from the experimental technique. Our method relies on the accurate recovery of the FRET decay parameters (see below), but is not limited by the slow time scale of NMR ($\sim 10^4$ times slower than fluorescence).

In the Theory section, it is shown that time-resolved FRET measurements can be used as a novel method to quantitate partition of probes in a biphasic lipid system and to estimate the phase boundary compositions for each temperature, and, ultimately, the phase diagram. However, Eqs. 13–14 and 18–21, which relate the decay parameters with the partition coefficients and the phase diagram information, are, on the whole, ill-conditioned, because of the divisions and subtractions involved in some of them, and also because the calculation of some parameters involves a "train" of equations, each contributing to error propagation.

This was the reason that led us to obtain synthetic FRET decays by Monte-Carlo techniques and compare the parameters recovered (after convoluting, adding noise, and analyzing the decays) with those used as input for the simulations. From comparison of the input and recovered parameters in Table 1, the results are largely satisfactory. Deviations in the recovered K_{pA} values are due to the small domain size, being much less important for 2500-molecule domains than for 400-molecule ones. A crucial part in the success of the present method is certainly played by the use of global analysis of the FRET decays (see e.g., Beechem et al., 1991 for a review on global analysis, or Loura et al., 1996 for a FRET application). If the donor–acceptor decays were analyzed alone, using Eq. 6, one would attempt to recover six different parameters (A_1, A_2, c_1, c_2, τ_1, τ_2) from a single decay curve. However, by analyzing the donor decay together with the respective donor–acceptor decay, three parameters become largely restricted (the lifetimes and the ratio A_1/A_2), leaving only the two acceptor concentrations and one pre-exponential factor to be completely optimized from a sole donor–acceptor decay. In this situation, the parameter recovery problem becomes certainly less critical than, e.g., for three-lifetime fitting, commonly used in protein and peptide fluorescence studies.

Of course, K_p values can be obtained by a plethora of established methods, including other photophysical techniques (Davenport, 1997). The uniqueness of FRET in this respect resides in the dependence of the "apparent K_p", the value recovered after analysis, on the size of the phases, as revealed from our simulations. Other fluorescent properties often used for calculation of K_p, like fluorescence intensity, lifetime, or anisotropy, are only dependent on the immediate environment of the probe (at least for common dyes, with lifetimes smaller than 10 ns), and are insensitive to the domain size. In this way, a procedure for obtaining information on the size of membrane domains would be the following:

i. Measure K_p by distance-independent methods;
ii. Obtain time-resolved FRET data and calculate K_{pA} from global analysis;
iii. Compare the K_{pA} values obtained in i. and ii. and, from their eventual difference, conclude about domain sizes;
iv. This would allow an "educated guess," which could in turn be confirmed from adequate Monte-Carlo simulations. Theoretical decay laws would thus be obtained and compared with the experimental ones.

EXPERIMENTAL

Materials

Cholesterol was purchased from Merck (Darmstadt, Germany). DMPC and the fluorescent species NBD-DMPE and Rh-DMPE were obtained from Avanti Polar Lipids (Birmingham, AL). All materials were used without further purification.

Vesicle preparation

Adequate amounts of stock solutions of host lipids and probes in chloroform and methanol, respectively, were mixed, dried until complete evaporation, and suspended in buffer (tris-HCl 50 mM, NaCl 100 mM, EDTA 0.2 mM, pH = 7.4; tris-HCl from BDH (London, U.K.) and NaCl and EDTA from Merck (Darmstadt, Germany) were used). Large unilamellar vesicles (LUV) were then prepared by the extrusion method (Hope et al., 1985). The probes were assumed to be symmetrically distributed between the two bilayer leaflets. For the FRET measurements, the NBD-DMPE and Rh-DMPE content in the vesicles was 0.1 and 0.5 mol%, respectively. To ensure that the lipid mixtures were in an equilibrium state, the prepared vesicles rested overnight at 25°C, and the measurements took place on the following day.

Instrumentation

Fluorescence decay measurements were carried out with a time-correlated single-photon counting system, which is described elsewhere (Loura et al., 2000). For the experiments at 30°C, time scales of 44.7 ps/ch and 34.0 ps/ch were used in the measurement of NBD-DMPE decays (excitation at 340 nm, emission at 520 nm) in the absence and presence of acceptor, respectively. For the experiments at 40°C, the time scales were 34.0 ps/ch in the measurement of NBD-DMPE decays in the absence of acceptor and

21.6 ps/ch in the presence of acceptor. For measurement of fluorescence decays of Rh-DMPE, the same instrument was used, but excitation was now at 570 nm using Rhodamine 6G as the laser dye, and emission was detected at 610 nm. The time scale was 15.3 ps/ch for measurements at both temperatures. Data analysis was carried out using a nonlinear, least squares iterative convolution method based on the Marquardt algorithm (Marquardt, 1963) using global analysis (e.g., Loura et al., 1996). The goodness of the fit was judged from the individual experiments' χ^2 values, global chi-square value, and weighted residuals and autocorrelation plots.

Fluorescence steady-state measurements were carried out with an SLM-Aminco 8100 Series 2 spectrofluorimeter (Rochester, NY; with double excitation and emission monochromators, MC-400) in a right-angle geometry. The light source was a 450-watt Xe arc lamp and the reference was a Rhodamine B quantum counter solution. Correction of excitation and emission spectra was performed using the apparatus correction software. 5 × 5-mm quartz cuvettes were used. Temperature was controlled to ±0.5°C by a thermostatted cuvette holder. Both emission and excitation spectral bandwidths were 4 nm.

The steady-state anisotropy, $\langle r \rangle$, was calculated from (Jabłoński, 1960)

$$\langle r \rangle = \frac{I_{VV} - G \cdot I_{VH}}{I_{VV} + 2 \cdot G \cdot I_{VH}}, \tag{24}$$

where the different intensities I_{ij} are the steady-state vertical and horizontal components of the fluorescence emission with excitation vertical (I_{VV} and I_{VH}, respectively) and horizontal (I_{HV} and I_{HH}, respectively) to the emission axis. The latter pair of components is used to calculate the G factor ($G = I_{HV}/I_{HH}$; Chen and Bowman, 1965). Polarization of excitation and emission light was achieved using Glan-Thompson polarizers. Absorption spectra were carried out in a Jasco V-560 spectrophotometer.

PROBE PHOTOPHYSICS AND PARTITION FROM NON-FRET MEASUREMENTS

NBD-DMPE

This probe shows biexponential decays for all studied samples. The longer recovered component measured 10–12 ns at $T = 30$°C and 8–10 ns at $T = 40$°C, depending on x_{chol}, with amplitude ~60–70%. The shorter and lesser component measured 1.9–2.2 ns at 30°C and 1.3–1.6 ns at 40°C. These values agree with those measured by Duportail et al. (1995), who also reported biexponential decays for the identical (with the same fluorophore, and just two additional methylene groups in each chain) *N*-(7-nitrobenz-2-oxa-1,3-diazol-4-yl)-dipalmitoylphosphatidylethanolamine (NBD-DPPE) probe in dipalmitoylphosphatidylglycerol vesicles.

A detailed study of the NBD-DMPE fluorescence decay was carried out as a function of x_{chol} (Fig. 2 *A*), revealing that $\bar{\tau}$ increases monotonously up to $x_{chol} = 0.28$, undergoes maxima for this composition both at 30 and 40°C, and decreases with further increase of cholesterol content. The maximum composition coincides with the $l_o + l_d$ tie-line end at 30°C (see Fig. 1), and differs slightly from this point at 40°C. From Fig. 1, it was expected that the composition for which there is a single l_o phase at 40°C would be ~31 mol%. Of course, as a consequence of Eq. 4, the decay for a sample in the phase coexistence range should be a linear combination of the decays in each pure phase, with coefficients proportional to the amount of probe in each phase. $\bar{\tau}$ should thus have a monotonous variation along the tie-line, and nonmonotonous variations have no physical meaning and are incompatible with global analysis (for optimization of lifetimes and donor pre-exponential ratios) of the decays. In this way, 28 mol% was taken as the composition for which the FRET decays are characteristic of pure l_o phase for both temperatures (instead of a higher value, e.g., 0.40, for which there would also be solely l_o phase, but with composition different from that in the coexistence region). Although this singularity was not observed at the opposite end of the tie-line, samples with $x_{chol} = 0.075$ and 0.14 were chosen (from the phase diagram, Fig. 1) as those for which the FRET decays are characteristic of pure l_d phase for 30 and 40°C, respectively (instead of, e.g., $x_{chol} = 0$).

Using as reference, the fluorescence quantum yield value Φ(NBD-DPPE) = 0.32 (Chattopadhyay, 1990), the values

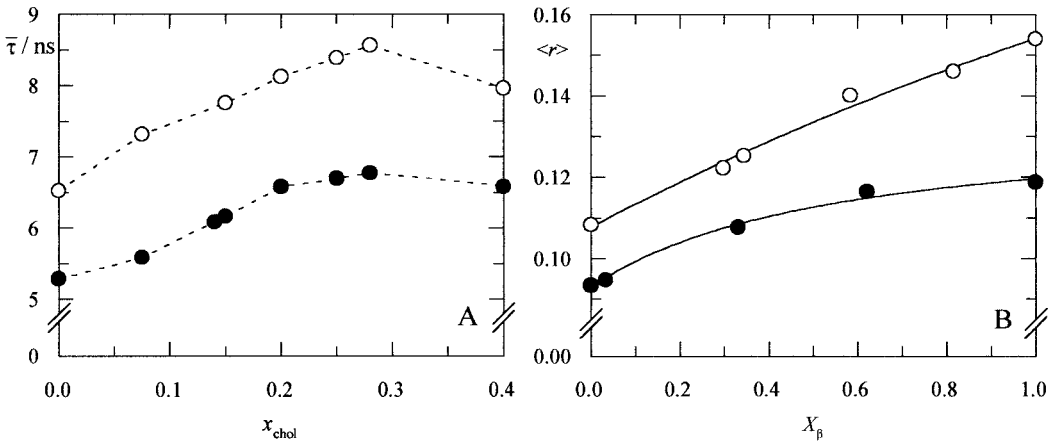

FIGURE 2 Variation of (*A*) average lifetime and (*B*) steady-state anisotropy of NBD-DMPE (0.1 mol%) in DMPC/cholesterol LUV, as a function of (*A*) global vesicle composition or (*B*) l_o phase fraction, for $T = 30$°C (○) and $T = 40$°C (●). The lines in *A* are mere guides to the eye, whereas the lines in *B* are fitting curves using Eqs. 12 and 25, with K_p (30°C) = 1.1 and K_p (40°C) = 2.6.

$\Phi(30°C, l_d) = 0.26$, $\Phi(30°C, l_o) = 0.29$, $\Phi(40°C, l_d) = 0.21$, and $\Phi(40°C, l_o) = 0.25$ were obtained. No major absorption or emission spectral or intensity alterations were apparent upon varying the cholesterol content of the vesicles. In this regard, the l_o/l_d partition coefficient for this probe, K_{pD}, was determined from fluorescence anisotropy measurements. Using Weber's law of additivity of anisotropy (Weber, 1952), the anisotropy in a l_o/l_d mixture is given by

$$\langle r \rangle = \frac{\varepsilon_\beta \cdot P_\beta \cdot \Phi_\beta \cdot g_\beta \cdot \langle r \rangle_\beta + \varepsilon_\alpha \cdot P_\alpha \cdot \Phi_\alpha \cdot g_\alpha \cdot \langle r \rangle_\alpha}{\varepsilon_\beta \cdot P_\beta \cdot \Phi_\beta \cdot g_\beta + \varepsilon_\alpha \cdot P_\alpha \cdot \Phi_\alpha \cdot g_\alpha}. \quad (25)$$

In Eq. 25, ε_i is the molar absorption coefficient, Φ_i is the fluorescence quantum yield, g_i is the fluorescence intensity at the emission wavelength in a normalized spectrum, for pure i phase, and P_i has the same meaning as in Eq. 12 (i = α or β for l_d and l_o, respectively). Assuming $\varepsilon_\alpha = \varepsilon_\beta$, $g_\alpha = g_\beta$, and $\Phi_\beta/\Phi_\alpha = \bar{\tau}_\beta/\bar{\tau}_\alpha$, and using $P_\beta/P_\alpha = K_p(1-X_\alpha)/X_\alpha$ (from Eq. 12), the only unknown parameter is K_p, which can be determined by fitting. This is shown in Fig. 2 *B*, and the values $K_{pD}(30°C) = 1.1$ and $K_{pD}(40°C) = 2.6$ are obtained.

Rh-DMPE

Rh-DMPE shows a significant decrease in fluorescence and absorption intensity with increasing cholesterol (results not shown). The absorption maximum undergoes a shift from $\lambda = 571$ nm ($x_{chol} = 0$) to $\lambda = 574$ nm ($x_{chol} = 0.28$). This latter value coincides with the absorption maximum in buffer. The absorption intensity in this medium is approximately half of that in the l_d phase and similar to that in the l_o phase. However, the shoulder observed in buffer at ~530 nm, indicating the presence of excitonic species, is not apparent in vesicles, even those with large x_{chol}. When x_{chol} increases from 0 to 0.40, emission intensity is reduced by 60%, but the spectra's shape is unchanged ($\lambda_{max} = 591$ nm).

Rh-DMPE decays are exponential up to $x_{chol} = 0.15$ at 30°C and 0.20 at 40°C ($\chi^2 < 1.2$), two exponentials being needed in the $x_{chol} = 0.20-0.25$ range, and three exponentials are necessary for $x_{chol} = 0.40$ for an adequate description (the new components are short-lived; result not shown). The fact that Rh-DMPE decays become gradually faster and more complex with increasing x_{chol} is probably due to an increased solvation of the lipid head groups for higher cholesterol content. This would result from steric restrictions imposed by cholesterol, which molecules would act as spacers between otherwise neighboring phospholipids, thus reducing the latter's intermolecular interactions and rendering their head groups more accessible to water, as verified by Ho et al. (1995). The increased polarity in the head group microenvironment also explains the shift of the absorption spectra.

Figure 3 shows the steady-state fluorescence intensity I_F and the lifetime averaged quantum yield $\bar{\tau}$ of Rh-DMPE as a function of the fraction of l_o in the vesicles, X_β. The variations of the two parameters are identical, and only for pure l_o small deviations between the relative values of I_F and $\bar{\tau}$ are detected. The fact that this discrepancy is verified solely for this sample and not for any other (not even for some samples characterized by a large X_β value) is related to either a poorer fitting of decay data or probably to the appearance of a static self-quenching component.

Contrary to NBD-DMPE, the steady-state anisotropy variation is not useful to study Rh-DMPE partition, because of the very efficient energy homotransfer among Rh-DMPE molecules, leading to strong emission depolarization. In this way, K_p should be calculated from the variation in I_F. The relationship between this parameter and the probe fraction

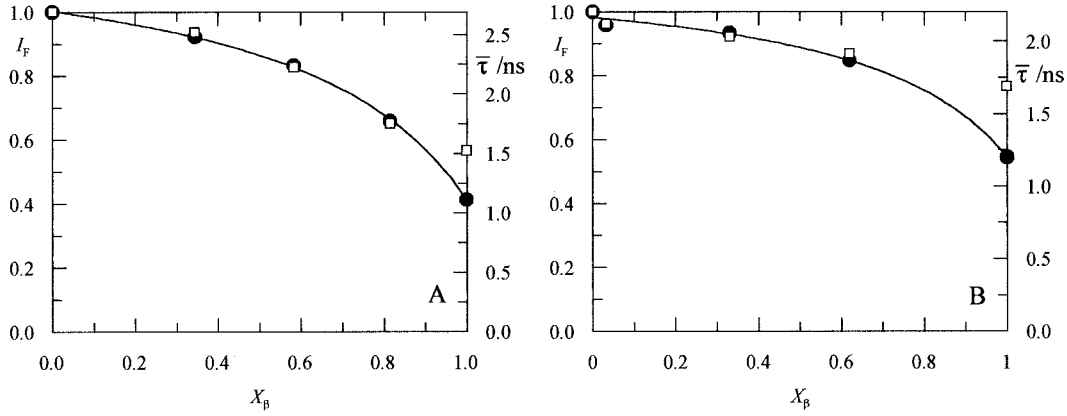

FIGURE 3 Variation of steady-state fluorescence intensity (I_F (a.u.); ●; $\lambda_{ex} = 560$ nm, $\lambda_{em} = 590$ nm) and average lifetime ($\bar{\tau}$; □) of Rh-DMPE as a function of l_o phase fraction (X_β), for (*A*) $T = 30°C$ and (*B*) $T = 40°C$. The curves are fits to I_F (Eqs. 12 and 26) with K_p (30°C) = 0.30 and K_p (40°C) = 0.27.

within each phase for dilute samples (total absorbency < 0.1) is given by (e.g., Ameloot et al., 1991)

$$I_F = K(P_\alpha \cdot \varepsilon_\alpha \cdot \Phi_\alpha + P_\beta \cdot \varepsilon_\beta \cdot \Phi_\beta), \quad (26)$$

where K includes a geometric factor and the intensity of inciding light. Using again $P_\beta/P_\alpha = K_p(1 - X_\alpha)/X_\alpha$, there are only two fitting variables, K and K_p. The curves in Fig. 3 were obtained this way, $K_p(30°C) = 0.30$ and $K_p(40°C) = 0.27$ being recovered. Thus, unlike NBD-DMPE, Rh-DMPE prefers unequivocally the l_d phase rather than the l_o phase, even tough the two probes have essentially the same lipid structure (only differing in the fluorescent label in the phospholipid head). This interesting difference is not readily explained.

FRET MEASUREMENTS AND DISCUSSION

From the spectral overlap of NBD-DMPE emission and Rh-DMPE absorption, as well as the donor fluorescence quantum yields (Φ_D) obtained above and the measured maximum molar absorption coefficient ε_{max}(Rh-DMPE, phase l_d) = $88 \times 10^3\ M^{-1}cm^{-1}$, the critical FRET distances R_0 were calculated using

$$R_0 = 0.2108[\kappa^2 \cdot \Phi_D \cdot n^{-4} \int_0^\infty I(\lambda) \cdot \varepsilon(\lambda) \cdot \lambda^4\, d\lambda]^{1/6}, \quad (27)$$

where κ^2 is the FRET orientation factor, n is the refractive index, and λ is the wavelength. κ^2 was taken as 5/4 (value for isotropic planar distribution of dipoles in the dynamic regime), the value used by Medhage et al. (1992) in their study of *N*-(lissamine™-rhodamine B)-dipalmitoylphosphatidylethanolamine (Rh-DPPE) energy migration in bilayers, while $n = 1.4$ was considered (Davenport et al., 1985). If the λ units used in Eq. 27 are nm, the calculated R_0 has Å units. The values obtained were $R_{0\alpha}$ (30°C) = 59.9 Å, $R_{0\alpha}$ (40°C) = 57.7 Å, $R_{0\beta}$ (30°C) = 61.1 Å, and $R_{0\beta}$ (40°C) = 59.4 Å.

Because both probes were mixed with adequate volumes of stock solutions of the host lipids, there is a bilayer geometry, and the decays should be analyzed using Eqs. 4, 5, 7, and 8. For this analysis, the interplanar distance in phase i, d_i, is required. Although the bilayer width varies with the cholesterol content (increases for T above the main transition temperature of the phospholipid, T_m; Ipsen et al., 1990), we did not find literature values for this effect in DMPC vesicles (the theoretical study of Ipsen et al. (1990) refers to DPPC). In any case, for DPPC at temperatures ~7°C above T_m and $x_{chol} = 0.25$, the bilayer width varies only 3 Å (visual inspection of Fig. 3 from Ipsen et al., 1990). In our study, this would be an approximation to T = 30°C and $x_{chol} = 0.25$, respectively, the lowest temperature and the highest cholesterol mole fraction studied inside the phase coexistence range. For larger T (40°C) or smaller x_{chol} (0.15, 0.20), the effect is even less pronounced. Because this variation in d_β is much smaller than R_0, a good approximation will certainly be to use the bilayer width for pure fluid DMPC, 35.5 Å (Marsh, 1990). This value should be increased by the distance between the Rh-DMPE chromophore and the lipid water interphase, which, according to Medhage et al. (1992), is ~3.5 Å. In contrast, the NBD-DMPE fluorophore is expected to be located at the interphase (Chattopadhyay and London, 1987). Therefore, the interplanar distance is taken as $d_\alpha = d_\beta = 39$ Å.

Table 2 shows the results of global analysis of the FRET decays. The energy transfer efficiency, E, calculated from the donor decays in absence and presence of acceptor ($\rho_D(t)$ and $\rho_{DA}(t)$, respectively), according to

$$E = 1 - \int_0^\infty \rho_{DA}(t)\, dt \Big/ \int_0^\infty \rho_D(t)\, dt, \quad (28)$$

is represented in Fig. 4 for both studied temperatures. From this figure it is clear that E decreases for both temperatures inside the phase coexistence range, and increases again (possibly not significantly for T = 40°C) at the phase coexistence limit. This happens because donor and acceptor

TABLE 2 Parameters of global analysis of FRET decays of the pair NBD-DMPE/Rh-DMPE in DMPC/cholesterol LUV

		x_{chol}					
Temperature	Parameter	0.075	0.14	0.15	0.20	0.25	0.28
30°C $\chi_G^2 = 1.56$	c_α	0.49	—	0.46	0.75	1.62	—
	c_β	—	—	0.41	0.39	0.35	0.37
	$q = A_\beta/A_\alpha$	—	—	0.58	2.13	5.45	—
	χ^2	1.80	—	1.48	1.43	1.43	1.69
40°C $\chi_G^2 = 1.46$	c_α	—	0.54	0.49	0.79	1.84	—
	c_β	—	—	0.27	0.45	0.44	0.46
	$q = A_\beta/A_\alpha$	—	—	0.051	1.60	4.26	—
	χ^2	—	1.41	1.46	1.35	1.35	1.75

For each composition, the presented χ^2 value is the average of the individual χ^2 in presence and absence of acceptor.
α denotes l_d phase and β denotes l_o phase.

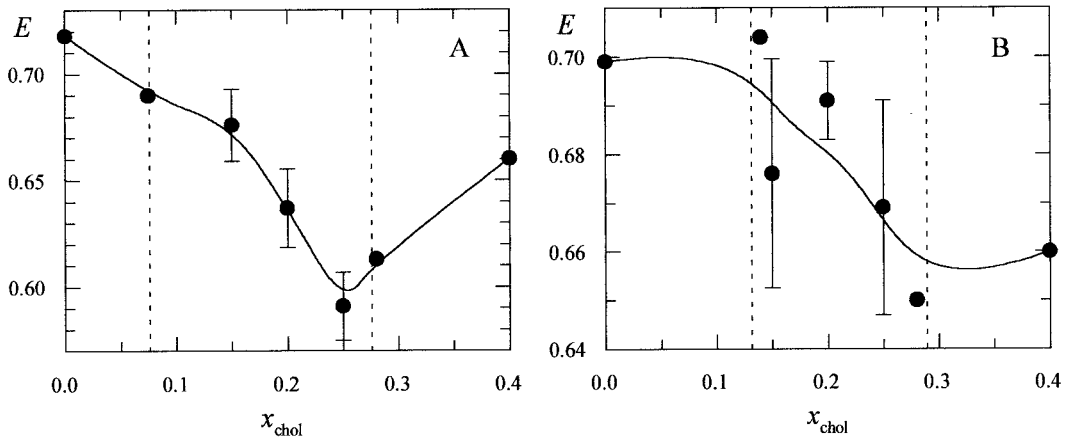

FIGURE 4 Variation of FRET efficiency of NBD-DMPE/Rh-DMPE in DMPC/cholesterol LUV, as a function of the cholesterol mole fraction, for (*A*) $T = 30°C$ and (*B*) $T = 40°C$. The error bars' extremes are the results of two different measurements. The dotted vertical lines represent the phase coexistence limits according to the phase diagram of Fig. 1.

have affinity for different phases, as was shown above. When phase separation occurs, the acceptor concentration around the majority of the donors is reduced, leading to less donor quenching and smaller E. For higher cholesterol concentration, there is a single phase again, and this compartmentalization effect disappears.

One can now apply the methodology presented above to calculate the apparent K_p values of both probes. For this system, Eqs. 13 and 14 should be written as

$$K_{pD}^{\beta/\alpha} = q(X_\alpha/X_\beta), \tag{29}$$

$$K_{pA}^{\beta/\alpha} = (c_\beta \cdot a_\beta)/(c_\alpha \cdot a_\alpha), \tag{30}$$

where c_i is proportional to the amount of acceptor in phase i (according to Eq. 3), a_i is the average area per lipid molecule in phase i, i = α or β for phase l_d or l_o (respectively), and q is the pre-exponential ratio A_α/A_β. q and c_i result directly from the decay analysis, whereas X_i (the molar fraction of phase i in the sample) comes from the phase diagram. As for a_α and a_β, one must take into account the bilayer condensation effect produced by cholesterol. In this way, the values of Smaby et al. (1997) obtained for non-ideal condensation in monolayers at 30 mN/m (Table 1 in this reference), together with those reported by Marsh (1990) for the area per DMPC molecule in pure bilayers (0.652 nm^2 at 30°C, 0.622 nm^2 at 40°C) are used to estimate a_α (30°C) = 0.601 nm^2, a_β (30°C) = 0.488 nm^2, a_α (40°C) = 0.535 nm^2, and a_β (40°C) = 0.452 nm^2. Table 3 shows the K_p values from Eqs. 29 and 30, which are compared with those obtained in the previous section from anisotropy or fluorescence intensity measurements.

Another interesting comparison is that of the experimental c_α and c_β values with the theoretical values. Using the K_{pA} values from steady-state fluorescence, for each composition X_β, the acceptor mole fraction inside each phase (P_β and $P_\alpha = 1 - P_\beta$) is calculated from Eq. 12, and used to calculate the surface acceptor concentration (n_i) according to

$$n_i = \frac{P_i \cdot F}{X_i \cdot a_i} \quad (i = \alpha, \beta), \tag{31}$$

where F is the bulk acceptor:lipid ratio, kept to 0.005 in our experiment. In turn, from n_i and Eq. 3, one obtains c_i. Figure 5 shows the theoretical and experimental c_i inside the phase coexistence range.

The results of Table 3 and Fig. 5 prompt the following considerations:

1. The donor partition coefficient values obtained from analysis of the decay data are very close to those obtained by anisotropy measurements. Considering a normal distribution of K_{pD} estimates, with 80% confidence level, one obtains K_{pD} (30°C) = 1.3 ± 0.3 and K_{pD} (40°C) = 2.4 ± 1.0. This proximity between FRET and anisotropy estimates of K_{pD} corresponds to the agree-

TABLE 3 Comparison of K_p values obtained from FRET global decay analysis (second, third, and fourth columns) with those obtained from variations of fluorescence anisotropy (K_{pD}) or fluorescence intensity (K_{pA})

	$x_{chol} = 0.15$	$x_{chol} = 0.20$	$x_{chol} = 0.25$	Values from r or I_F
30°C				
K_{pD}	1.1	1.5	1.2	1.1
K_{pA}	0.73	0.42	0.18	0.30
40°C				
K_{pD}	1.5	3.2	2.6	2.6
K_{pA}	0.47	0.49	0.20	0.27

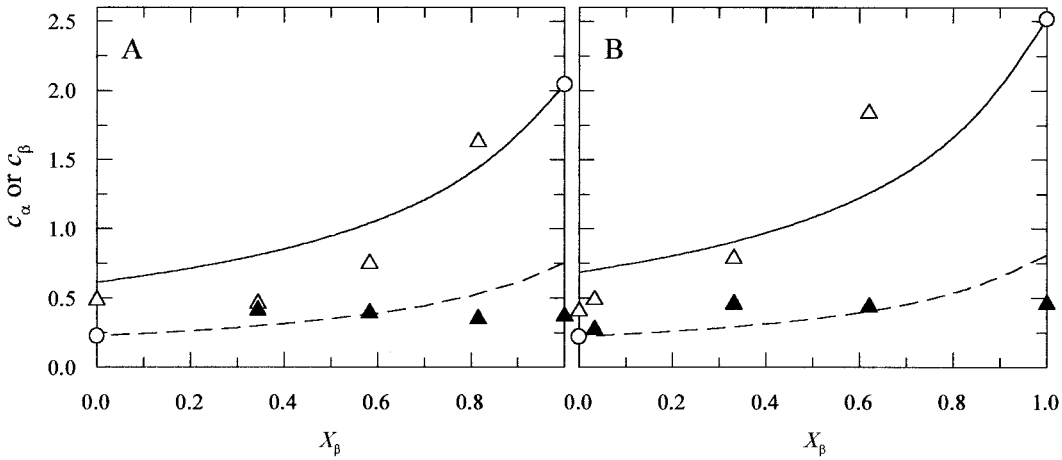

FIGURE 5 Theoretical values (—— and – – –, respectively) and experimental fitting values (△ and ▲, respectively) for c_α and c_β, the c parameters (proportional to acceptor concentration) associated to l_o and l_d phases (respectively) for NBD-DMPE/Rh-DMPE in DMPC/cholesterol LUV. The open circles represent points where one of the functions c_α or c_β is not defined. (*A*) $T = 30°C$; (*B*) $T = 40°C$.

ment of input and recovered K_{pD} values in the Simulations section (see Table 1).

2. Turning our attention now to K_{pA}, the values obtained for the samples with 25 mol% are the ones closest to those obtained from I_F variation. The fact that the apparent FRET K_{pA} are somewhat smaller than the K_{pA} obtained from I_F for this composition at both temperatures could result from several factors. One hypothesis, suggested by the decrease of absorption and emission intensity, is the existence of a certain degree of acceptor aggregation in the l_o phase. This would indeed lead to a negative error in the recovered c_β, and, consequently, K_{pA} (Eq. 29). In any case, note that, for Rh-DMPE, there is little static fluorescence self-quenching in that phase, which could mean that this effect is not too significant. Moreover, despite the reduction in absorption intensity, the spectra shape remains the same, apart from a small bathochromatic shift. In particular, the shoulder at ~535 nm is not enhanced (as observed in buffer, where there is certainly substantial Rh-DMPE aggregation). Another equally probable hypothesis is the uncertainty associated to the used a_α and a_β values. Still, the agreement between the K_{pA} recovered from the FRET formalism for the sample with $x_{chol} = 0.25$ and the values obtained from I_F measurements is quite reasonable.
3. An equivalent point is the proximity between the c_i recovered from FRET analysis of experimental decays and the theoretical curves for $x_{chol} = 0.25$ (the sample with the larger l_o phase fraction X_β inside the l_o/l_d coexistence range). The fact that the experimental c_α is larger than expected (especially for $T = 40°C$) may be due to one of the factors mentioned above, or to inaccuracy in the theoretical curves (which would occur if the experimental acceptor:total lipid ratio were not exactly 0.005, or if there were errors in the K_{pA} calculated from I_F measurements), or probably to the difficulty in recovery of the correct FRET decay fitting parameters, due to their correlation. In any case, an identical tendency, described below, is clear for both studied temperatures.

The FRET recovered apparent K_{pA} value decreases from the sample with $x_{chol} = 0.15$ to that with $x_{chol} = 0.20$ at 30°C (being invariant at 40°C), and from the latter to that with $x_{chol} = 0.25$ at both temperatures. The fact that, for $x_{chol} = 0.15$ and $x_{chol} = 0.20$, one recovers FRET k_{pA} values larger than those measured from I_F measurements is not due to aggregation in either the l_o phase (which would have the opposite effect) or the l_d phase (which is similar to pure phospholipid fluid phase, in which the probes disperse randomly; Loura et al., 1996). Figure 5 suggests the most probable cause for this observation. For $x_{chol} = 0.15$ and $x_{chol} = 0.20$ (the studied samples with smaller X_β in the l_o/l_d coexistence range), the experimental c_α value (which would always be expected to be larger than c_β, according to the K_{pA} calculated from I_F measurements) is smaller than expected, whereas the opposite is true for c_β. This behavior recalls the Monte-Carlo simulations, which showed that FRET K_{pA} values closer to unity than expected from the input distributions are recovered due to the existence of small domains of the minor phase.

At this point, it is interesting to compare the relative deviations between the FRET-recovered K_{pA} and the theoretical values (for the simulations) or the I_F-recovered values (for the experimental study). Note that both the theoretical K_{pA} values and those obtained experimentally from I_F measurements are the "real" K_{pA} values, unaffected by the domain size of the coexistence phases, whereas the FRET-recovered value, as shown in the Simulations section, is sensitive to this variable. In these studies, the average relative deviation in K_{pA} (excluding the simulations which

had homogeneous distributions of acceptors) is 27% for domains of size ≈3.5 R_0 and 10% for domains of size ≈9 R_0. The deviations for the present study, calculated from $100\% \times |K_{pA}(\text{FRET}) - K_{pA}(I_F)|/K_{pA}(I_F)$, are 143% ($T$ = 30°C, x_{chol} = 0.15), 40% (T = 30°C, x_{chol} = 0.20), 74% (T = 40°C, x_{chol} = 0.15), and 81% (T = 40°C, x_{chol} = 0.20).

These numbers should be viewed cautiously, because there is not exact matching between input simulation variables and the experimental parameters, and the simulated domains had a shape and size distribution that probably differs from the actual ones, but they clearly indicate the following:

- In the systems that have smaller amount of l_o phase (x_{chol} = 0.15 and 0.20 for T = 40°C, x_{chol} = 0.15 for T = 30°C), the considerable deviation between K_{pA} (FRET) and $K_{pA}(I_F)$ suggests that the l_o domains, dispersed in l_d phase, should be very small, of the order of magnitude of R_0, that is, a few nm. The fact that these deviations are much larger than those calculated for simulations for domain size 3.5 R_0 (~20–25 nm for this system) indicates that the l_o domains should be smaller than this value.
- This effect is apparently more important for T = 30°C than for T = 40°C. In fact, for T = 30°C, the acceptor concentrations in the two phases are very close (implying very small domains) even for an X_β value as large as ~0.3 (for x_{chol} = 0.15). Regarding T = 40°C, even for X_β as low as ~4 mol% (for x_{chol} = 0.15), the two concentrations are very different, even if none reaches the respective theoretical value.
- On the contrary, when the least abundant phase is l_d, the domains of this phase should be much larger than R_0 (at least for $X_\alpha = 1 - X_\beta \approx 0.2$), because the FRET-recovered K_{pA} values show small negative deviations relative to the I_F derived ones. The reason for these deviations was discussed above, and is surely not compartmentalization in small domains (which effect would be the opposite).

In this discussion, we have so far assumed that the DMPC/cholesterol mixture phase behavior is explained by the phase diagram of Fig. 1. Of course, as shown in the Theory section (see Eqs. 18–21), one of the major advantages of the FRET formalism for partition of probes in a biphasic system is that it does not require a priori knowledge of the phase diagram, because its limits x_α (composition for which X_α = 1) and x_β (composition for which X_β = 1) are determined from the same experiment. Strictly, the equations used should be valid for large domains. In practice, as shown in the simulations in the preceding paper, relatively accurate recovery of the diagram limits is still possible for domain sizes of ~3.5 R_0. For this purpose, two points inside the phase coexistence range are needed. We chose the two higher cholesterol concentrations (x_{chol} = 0.20 and x_{chol} = 0.25), because, as discussed above, for x_{chol} = 0.15 the l_o domains are very small.

Table 4 shows the results of this analysis. The most striking feature is the fact that, at T = 30°C, the l_d fraction X_α is significantly larger than predicted by the phase diagram. For x_{chol} = 0.20 l_d is predicted to be the most abundant phase, contrary to the phase diagram. Ultimately, the consequence of this is the calculation of a coexistence limit value x_α larger than that of the published diagram limit for both temperatures. Naturally, these results should be considered with caution, because of the error propagation associated with the equations used. However, they are entirely consistent with the preceding discussion. The result $x_\alpha > 0.15$ means that FRET is unable to detect phase separation for the x_{chol} = 0.15 sample, because the perceived domains are too small. Bear in mind that the sensed concentrations c_α and c_β are almost equal for this concentration, not because acceptor partition is almost indifferent for this composition (Rh-DMPE shows a marked preference for the l_d phase, as shown by the photophysical study of this probe), but because the domains are so small that all donors, irrespective of the phase in which they are located, sense acceptors from both environments, and are practically equivalent. Thus, these results do not necessarily contradict the published diagram, which was also confirmed by domain size-independent fluorescent measurements (*trans*-parinaric acid fluorescence; Mateo et al., 1995). They stem from the distance dependence of FRET and the existence of small domains. In other words, there may be phase separation below $x_\alpha < 0.15$, but, if this is the case, the domains should be very small. Ideally, the published and FRET coexistence boundaries should coincide if the phases are large. That is observed at the other end of the tie-line, for

TABLE 4 l_o and l_d phase fractions (X_α and X_β, respectively) and phase diagram limits (x_α: x_{chol} when X_α = 1; x_β: x_{chol} when X_β = 1) calculated from the FRET global decay parameters of the samples with x_{chol} = 0.20 and 0.25

T/°C	30		40	
x_{chol}	0.20	0.25	0.20	0.25
X_α	0.778 (0.390)	0.276 (0.146)	0.844 (0.647)	0.245 (0.353)
X_β	0.222 (0.610)	0.724 (0.854)	0.156 (0.353)	0.755 (0.647)
x_α	0.178 (0.075)		0.187 (0.14)	
x_β	0.277 (0.28)		0.270 (0.31)	

which the accordance between the FRET-recovered and the published x_β is very good.

CONCLUSION

It is important to stress that the present study does not allow precise estimation of domain size values or distributions. However, they do set upper limits for the domain size of l_o phase, which should be very small, especially for $T = 30°C$. A justification of this fact in terms of the properties of the coexisting phases or the biological role of cholesterol is clearly not immediate. A likely possibility is that these observations are related to different processes of phase separation. The fact that apparently equilibrated l_d-rich samples have small l_o domains suggests that formation of l_o phase from initially pure l_d (which could be induced by lowering temperature or relative cholesterol enrichment) occurs mainly by nucleation of small l_o domains which do not coalesce appreciably into large domains even for large overall l_o fraction (~0.3 at 30°C). Conversely, formation of l_d phase from pure l_o samples (resulting from temperature increase or relative phosphatidylcholine enrichment) probably occurs preferably by growth of a smaller number of domains. Pralle et al. (2000), using single-particle tracking, recently reported 26 ± 13 nm (inside the range of the FRET interaction) as the size of sphingolipid-cholesterol rafts, a value of the same order of magnitude of the cholesterol-rich domains detected in this study of DMPC/cholesterol bilayers.

These results illustrate the possibility of detection of microdomains by the means of FRET global decay analysis, necessarily in conjunction with other techniques capable of measuring the acceptor partition coefficient independently of the domain size. One can easily devise experiments in which this methodology can be applied for systems closer to biomembranes in their complexity (for which this type of information will certainly have large importance). A FRET approach (but microscopic rather than spectroscopic, and necessarily less quantitative) was recently taken by Kenworthy and Edidin (1998) in their imaging study of the distribution of a glycosylphosphatidylinositol-anchored protein at the apical surface of MDCK cells, illustrating the potential of FRET in the study of microheterogeneity in natural membranes.

This work was supported by PRAXIS XXI (Ministério da Ciência e Tecnologia, Portugal), project PRAXIS/P/SAU/14025/1998.

REFERENCES

Almeida, P. F. F., W. L. C. Vaz, and T. E. Thompson. 1992. Lateral diffusion in the liquid phases of dimirystoylphosphatidylcholine/cholesterol bilayers: a free volume analysis. *Biochemistry.* 31: 6739–6747.

Almeida, P. F. F., W. L. C. Vaz, and T. E. Thompson. 1993. Percolation and diffusion in three component lipid bilayers: effect of cholesterol on an equimolar mixture of two phosphatidylcholines. *Biophys. J.* 64: 399–412.

Ameloot, M., N. Boens, R. Andriessen, V. Van der Bergh, and F. C. De Schryver. 1991. Non *a priori* analysis of fluorescence decay surfaces of excited-state processes. 1. Theory. *J. Phys. Chem.* 95:2041–2047.

Beechem, J. M., E. Gratton, M. Ameloot, J. R. Knutson, and L. Brand. 1991. The global analysis of fluorescence intensity and anisotropy decay data: second-generation theory and programs. *In* Topics in Fluorescence Spectroscopy, Vol. 2: Principles. J. R. Lakowicz, editor. Plenum Press, New York. 241–305.

Chattopadhyay, A., and E. London. 1987. Parallax method for direct measurement of membrane penetration depth utilizing fluorescence quenching by spin-labeled phospholipids. *Biochemistry.* 26:39–45.

Chattopadhyay, A. 1990. Chemistry and biology of *N*-(7-nitrobenz-2-oxa-1,3-diazol-4-yl)-labeled lipids: fluorescent probes of biological and model membranes. *Chem. Phys. Lipids.* 53:1–15.

Chen, R., and R. L. Bowman. 1965. Fluorescence polarization: measurement with ultraviolet-polarizing filters in a spectrophotofluorometer. *Science.* 147:729–732.

Davenport, L., R. E. Dale, R. H. Bisby, and R. B. Cundall. 1985. Transverse location of the fluorescent probe 1,6-diphenyl-1,3,5-hexatriene in model lipid bilayer membrane systems by resonance energy transfer. *Biochemistry.* 24:4097–4108.

Davenport, L. 1997. Fluorescence probes for studying membrane heterogeneity. *Methods Enzymol.* 278:487–512.

Duportail, G., F. Merola, and P. Lianos. 1995. Fluorescence energy transfer in lipid vesicles. A time-resolved analysis using stretched exponentials. *J. Photochem. Photobiol. A: Chem.* 89:135–140.

Edidin, M. 1997. Lipid microdomains in cell surface membranes. *Curr. Opin. Struct. Biol.* 7:528–532.

Förster, T. 1949. Experimentelle und theoretische Untersuchung des Zwischenenmolekularen übergangs von Elektronenanregungserenrgie. *x. Naturforsch.* 4a:321–327.

Gabdoulline, R. R., G. Vanderkooi, and C. Zheng. 1996. Comparison of the structures of dimyristoylphosphatidylcholine in the presence and absence of cholesterol by molecular dynamics simulations. *J. Phys. Chem.* 100:15942–15946.

Hauser, M., U. K. A. Klein, and U. Gösele. 1976. Extension of Förster's theory of long range energy transfer to donor–acceptor pairs in systems of molecular dimensions. *Z. Phys. Chem.* 101:255–266.

Ho, C., S. J. Slater, and C. D. Stubbs. 1995. Hydration and order in lipid bilayers. *Biochemistry.* 34:6188–6195.

Hope, M. R., M. B. Bally, G. Webb, and P. R. Cullis. 1985. Production of large unilamellar vesicles by a rapid extrusion procedure. Characterization of size distribution, trapped volume and ability to maintain a membrane potential. *Biochim. Biophys. Acta.* 812:55–65.

Ipsen, J. H., O. G. Mouritsen, and M. Bloom. 1990. Relationships between lipid membrane area, hydrophobic thickness, and acyl-chain orientational order. The effects of cholesterol. *Biophys. J.* 57:405–412.

Jabłoński, A. 1960. On the notion of emission anisotropy. *Bull. Acad. Pol. Sci.* 8:259–264.

Kenworthy, A. K., and M. Edidin. 1998. Distribution of a glycosylphosphatidylinositol-anchored protein at the apical surface of MDCK cells examined at a resolution of <100 Å using imaging fluorescence resonance energy transfer. *J. Cell. Biol.* 142:69–84.

Lafleur, M., P. R. Cullis, and M. Bloom. 1990. Modulation of the orientational order profile of the lipid acyl chain in the L alpha phase. *Eur. Biophys. J.* 19:55–62.

Lakowicz, J. R. 1999. Principles of Fluorescence Spectroscopy. 2nd ed. Kluwer Academic/Plenum Press, New York. Chap. 13–15.

Lentz, B. R., D. A. Barrow, and M. Hoechli. 1980. Cholesterol–phosphatidylcholine interactions in multilamellar vesicles. *Biochemistry.* 19: 1943–1954.

Loura, L. M. S., A. Fedorov, and M. Prieto. 1996. Resonance energy transfer in a model system of membranes: application to gel and liquid crystalline phases. *Biophys. J.* 71:1823–1836.

Loura, L. M. S., Fedorov, and M. Prieto. 2000. Membrane probe distribution heterogeneity: a resonance energy transfer study. *J. Phys. Chem. B.* 104:6920–6931.

Mabrey, S., P. L. Mateo, and J. M. Sturtevant. 1978. High-sensitivity scanning calorimetric study of mixtures of cholesterol with dimyristoyl- and dipalmitoyl-phosphatidylcholines. *Biochemistry.* 17:2464–2468.

Marquardt, D. W. 1963. An algorithm for least-squares estimation of non-linear parameters. *J. Soc. Ind. Appl. Math. (SIAM J.).* 11:431–441.

Marsh, D. 1990. Handbook of Lipid Bilayers. CRC Press, Boca Raton, FL.

Mateo, C. R., A. U. Acuña, and J.-C. Brochon. 1995. Liquid-crystalline phases of cholesterol/lipid bilayers as revealed by the fluorescence of *trans*-parinaric acid. *Biophys. J.* 68:978–987.

McMullen, T. P. W., and R. N. McElhaney. 1996. Physical studies of cholesterol–phospholipid interactions. *Curr. Opin. Colloid Interface Sci.* 1:83–90.

Medhage, B., E. Mukhtar, B. Kalman, L. B.-Å. Johansson, and J. G. Molotkovsky. 1992. Electronic energy transfer in anisotropic systems. 5. Rhodamine-lipid derivatives in model membranes. *J. Chem. Soc. Faraday Trans.* 88:2845–2851.

Méléard, P., C. Gerbeaud, T. Pott, L. Fernandez-Puente, I. Bivas, M. D. Mitov, J. Dufourcq, and P. Bothorel. 1997. Bending elasticities of model membranes: influences of temperature and sterol content. *Biophys. J.* 72:2616–2629.

Pralle, A., P. Keller, E. Florin, K. Simons, and J. K. Horber. 2000. Sphingolipid-cholesterol rafts diffuse as small entities in the membrane of mammalian cells. *J. Cell. Biol.* 148:997–1008.

Robinson, A. J., W. G. Richards, P. J. Thomas, and M. M. Hann. 1995. Behavior of cholesterol and its effect on headgroup and chain conformations in lipid bilayers: a molecular dynamics study. *Biophys. J.* 68:164–170.

Sankaram, M. B., and T. E. Thompson. 1990. Modulation of phospholipid acyl chain order by cholesterol. A solid-state ^{2}H nuclear magnetic resonance study. *Biochemistry.* 29:10676–10684.

Sankaram, M. B., and T. E. Thompson. 1991. Cholesterol-induced fluid phase immiscibility in membranes. *Proc. Natl. Acad. Sci. USA.* 88: 8686–8690.

Sankaram, M. B., D. Marsh, and T. E. Thompson. 1992. Determination of fluid and gel domain sizes in two-component, two-phase bilayers. An ESR spin label study. *Biophys. J.* 63:340–349.

Smaby, J. M., M. M. Momsen, H. L. Brockman, and R. E. Brown. 1997. Phosphatidylcholine acyl unsaturation modulates the decrease in interfacial elasticity induced by cholesterol. *Biophys. J.* 73:1492–1505.

Smondyrev, A. M., and M. L. Berkowitz. 1999. Structure of dipalmitoylphosphatidylcholine/cholesterol bilayer at low and high cholesterol concentrations: molecular dynamics simulation. *Biophys. J.* 77: 2075–2089.

Snyder, B., and E. Freire. 1982. Fluorescence energy transfer in two dimensions. A numeric solution for random and non-random distributions. *Biophys. J.* 40:137–148.

Stryer, L. 1978. Fluorescence energy transfer as a spectroscopy ruler. *Ann. Rev. Biochem.* 47:819–846.

Tu, K., M. L. Klein, and D. L. Tobias. 1998. Constant-pressure molecular dynamics investigation of cholesterol effects in a dipalmitoylphosphatidylcholine bilayer. *Biophys. J.* 75:2147–2156.

Vanderkooi, G. 1994. Computation of mixed phosphatidylcholine– cholesterol bilayer structures by energy minimization. *Biophys. J.* 66:1457–1468.

Van Der Meer, B., G. Coker, III, and S.-Y. S. Chen. 1994. Resonance Energy Transfer: Theory and Data. VCH Publishers, New York.

Vist, M. R., and J. H. Davis. 1990. Phase equilibria of cholesterol/DPPC mixtures: ^{2}H-NMR and differential scanning calorimetry. *Biochemistry.* 29:451–464.

Weber, G. 1952. Polarization of the fluorescence of macromolecules. I. Theory and experimental method. *Biochem. J.* 51:145–155.

Xiang, T.-X., and B. D. Anderson. 1997. Permeability of acetic acid across gel and liquid–crystalline lipid bilayers conforms to free-surface-area theory. *Biophys. J.* 72:223–237.